

QUENCHING OF A HEATED ROD: PHYSICAL PHENOMENA AND HEAT TRANSFER

Arnab Dasgupta, P. P. Kulkarni, G.J. Gorade, D.K. Chandraker, A.K. Nayak, P.K. Vijayan

Reactor Engineering Division
Bhabha Atomic Research Centre, Mumbai, India
arnie@barc.gov.in, parimalk@barc.gov.in, gjgorade@barc.gov.in, dineshkc@barc.gov.in,
arunths@barc.gov.in, vijayanp@barc.gov.in

S.P. Walker
Dept. of Mechanical Engineering,
Imperial College, London, United Kingdom
s.p.walker@imperial.ac.uk

ABSTRACT

The physical phenomena of rewetting and quenching are of prime importance in nuclear reactor safety in event of a Loss of Coolant Accident (LOCA). Generally, top spray or bottom flooding concepts are used in reactors. Numerical simulation of these processes entails the use of the concept of a rewetting velocity. However, heat transfer just before and after the rewetting front is often assumed in an ad-hoc fashion. The present work aims to evaluate the surface heat flux during rewetting and quenching process as a function of surface temperature.

The experiments presented herein are primarily applicable to the bottom flooding scenario with high flooding rate. In the experiments, a rod heated above Leidenfrost point is immersed in a pool of water. The surface temperature was recorded using a surface mounted thermocouple. The surface heat flux was then determined numerically and hence can be related to a particular value of surface temperature. This type of data is useful for numerical simulations of quenching phenomena. In addition to this, high speed photography was undertaken to visualize the phenomena taking place during quenching. Both subcooled and saturated water pools have been used and compared in the experiments.

KEYWORDS

Rewetting, Quenching, Heat-flux, Surface temperature

1. INTRODUCTION

The cooling of fuel pins after a Loss of Coolant Accident (LOCA) is essential to ensure safety of any nuclear reactor. In water cooled reactors, the cooling is achieved by injecting Emergency Core Cooling (ECC) water into the core. The fuel in such circumstances is already heated to temperatures higher than Leidenfrost point and the water is initially unable to wet the clad surface. Thus heat transfer begins in the film boiling regime. As cooling proceeds, different regimes of boiling are encountered. The prediction of heat transfer and knowledge of physical processes occurring is important for safety case analysis.

Two types of phenomena can occur depending on the rate of flooding (fig. 1). For the low flooding rate case, annular flow is observed with the progress of the liquid film indicating progress of wetting front and rewetting velocity. With high flooding rate, the water fills up faster than it can wet and a vapor film is formed. Boiling with this type of phase distribution is called Inverted Annular Film Boiling (IAFB). The present experiments are closer to the second phenomenon. It is appropriate at this point to specify that during reflooding, rewetting corresponds to the first establishment of water contact with the surface and quenching corresponds to the point wherein the surface temperature has dropped substantially. The idea of quenching is made clearer in section 4 where quenching time is quantified.

The motivation for the present experiments is to characterize the surface heat flux as a function of surface temperature. Such a characterization is important particularly for the transition boiling regime where in spite of many studies[1], there exist few models or correlations.

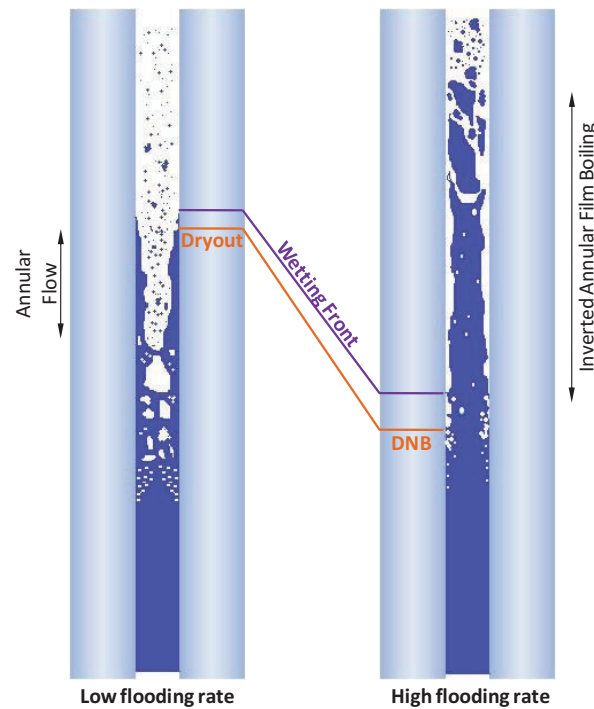


Figure 1. Heat transfer mechanisms during reflooding [2]

Earlier studies of similar nature have been performed in channels [3,4]. In those cases reflooding was simulated and thus the evaluation of surface heat flux became a two-dimensional problem. Experiments based on the immersion technique have been done on metal spheres [5] and heated rodlets [6,7]. In those cases however, the temperature is measured inside the heated sample and a lumped capacitance model is assumed to evaluate the heat flux from temperature record. Thus though, the heat flux is obtained as a function of temperature, it cannot be truly labeled as surface temperature, which is of prime importance during rewetting. There are many other studies on falling films which have been nicely described by Walker et al. [8]. Walker et al. [8] have also observed using high speed photography, many micro scale wettings prior to complete wetting of the surface. However their technique does not allow surface heat flux evaluation.

The present experiment allows the surface temperature measurements and a scheme to evaluate surface heat flux. The next section describes the quenching experiment performed. This is followed by a discussion on the mathematical technique used to derive the surface heat flux from the surface

temperature versus time data. The results are given in section 4 and the outcomes are concluded in section 5.

2. EXPERIMENT

The experiments involved quenching of a heated rod in a pool of water (Fig. 2). A 0.5mm sheathed thermocouple (accuracy: $\pm 0.4\%$ of reading) was brazed to the pin surface for surface temperature measurement. The measurement was done at around the middle of the rod length to avoid end effects. The brazing procedure to ensure measurement of surface temperature is described in greater detail by Vishnoi et al.[9]. Another thermocouple was placed diametrically opposite and axially offset by 30 mm from the first thermocouple. This second thermocouple was kept to check the effect (if any!) of axial conduction. The temperatures were recorded using Yokogawa DX1004 data acquisition system with a recording speed of 40 Hz. The boiling phenomena occurring in water pool were visualized using fast camera (make: Mikrotron Motionblitz cube 8) at a frame rate of 800 Hz.

The temperature-time traces of the two thermocouples, from the time they first came into contact with water, were seen to be overlap (within experimental accuracy). This ensured that the quenching behavior was indeed same at different axial locations and neglect of axial conduction would not cause major errors in surface heat flux estimation (section 3).

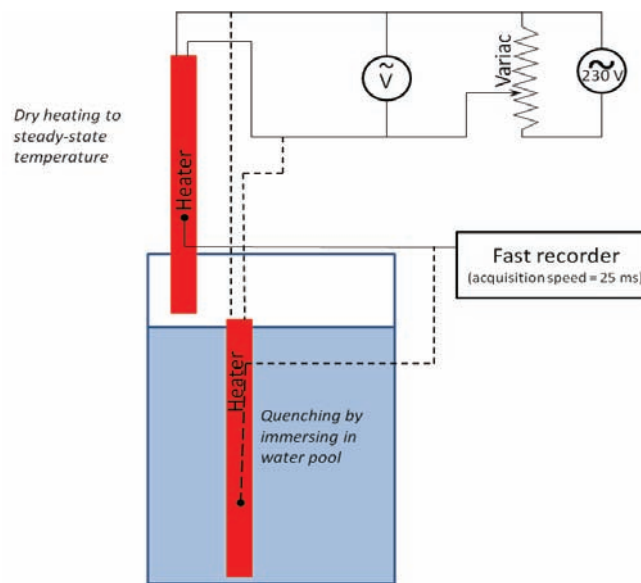


Figure 2. Schematic of experimental setup

The heater rod used was a cartridge type electrical heater with rated power of 800W and electrical resistance of 76Ω . The outer diameter of the rod was 12.7 mm and length was 254mm. The heating element (nichrome) was contained in compacted Magnesium Oxide core. The outer sheath (0.5 mm) of the heater was made of stainless steel 304. The applied voltage to the heater could be varied using a Variac. The applied voltage was measured using a digital volt meter.

For the experiments, the rod was first heated in air to achieve a steady state surface temperature of $\sim 460^\circ\text{C}$. This usually required putting in much lesser than rated power. Once steady state conditions were attained, the power was turned off and heater immediately immersed in the water pool. The temperature of the pool was measured using mercury thermometer. The cases experimented upon are tabulated in table I.

Table I Experiment matrix

S. No.	Fluid in pool	Temperature	Photography
1	Water	100°C (saturated)	Yes
2.	Water	25°C (subcooled)	Yes

3. MATHEMATICAL MODEL FOR SURFACE HEAT FLUX DETERMINATION

The mathematical analysis for the experiment described above falls in the class of inverse heat conduction problems. While in conventional problems, the heat flux is known and the resulting temperature distribution is evaluated, in this case, the heat flux has to be derived from temperature measurement. In fact, rewetting and quenching phenomena are governed by the surface temperature and heat flux is a dependent variable. The inverse heat transfer problem thus adequately represents the physics of the process.

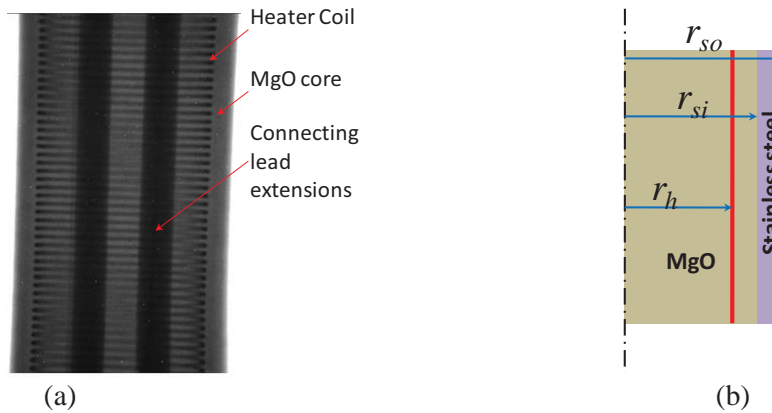


Figure 3. (a) Radiograph of the heater and (b) assumed schematic for modeling

The model is based on two experimental inputs; firstly the input power and surface temperature at steady state conditions and secondly, the surface temperature record through the thermocouple. The steady-state values of surface temperature and heater power are used to evaluate the temperature profile within the cylindrical heater (eqn. 1).

$$\begin{aligned}
 &= -\frac{q_{tot}}{2\pi L k_{MgO}} \ln\left(\frac{r_h}{r_{si}}\right) + T(r_{si}) \quad r < r_h \\
 T(r) &= -\frac{q_{tot}}{2\pi L k_{MgO}} \ln\left(\frac{r}{r_{si}}\right) + T(r_{si}) \quad r_h < r < r_{si} \\
 &= -\frac{q_{tot}}{2\pi L k_{SS}} \ln\left(\frac{r}{r_{so}}\right) + T(r_{so}) \quad r_{si} \leq r \leq r_{so}
 \end{aligned} \tag{1}$$

$$\frac{\partial T}{\partial t} = \frac{1}{r} \frac{\partial}{\partial r} \left(\alpha r \frac{\partial T}{\partial r} \right) \tag{2}$$

Of course the heater internals have to be considered to derive this profile. The heater internal structure was approximated through X-ray radiography (fig. 3). In the mathematical model, the heater coil is

treated as a thin constant heat source generating q_{tot} over a length L at a radius of r_h . The connecting lead extensions do not generate any heat and have been neglected in the model. The transient surface temperature data during quenching is used as a time dependent boundary condition for the solution of the 1-D transient conduction equation (eqn. 2), to derive the temperature gradient in the heater. Since eqn. (2) is second order in r , another radial boundary condition is required. This is obtained by considering symmetry of the cylinder i.e., the radial temperature gradient is zero at centre line. The initial condition for solution of eqn. (2) is obtained from eqn. (1).

The thermal conductivity, k has subscripts MgO and SS denoting magnesium oxide and stainless steel respectively. The thermal diffusivity, α was also changed accordingly while solving the quenching transient. Since the complete heater is immersed in water nearly instantaneously, the axial conduction effects are neglected and the surface heat flux can be obtained from a single thermocouple reading.

4. RESULTS

The results are presented in two forms – the raw results of temperature versus time (or quenching curves) are given in section 4.1 and computed results on heat flux are given in section 4.2.

4.1. Quenching Curves

4.1.1. Saturated pool

The results for the saturated pool and associated photographs of the phenomena are given in figure. 4. The green dot represents the location of the surface thermocouple.

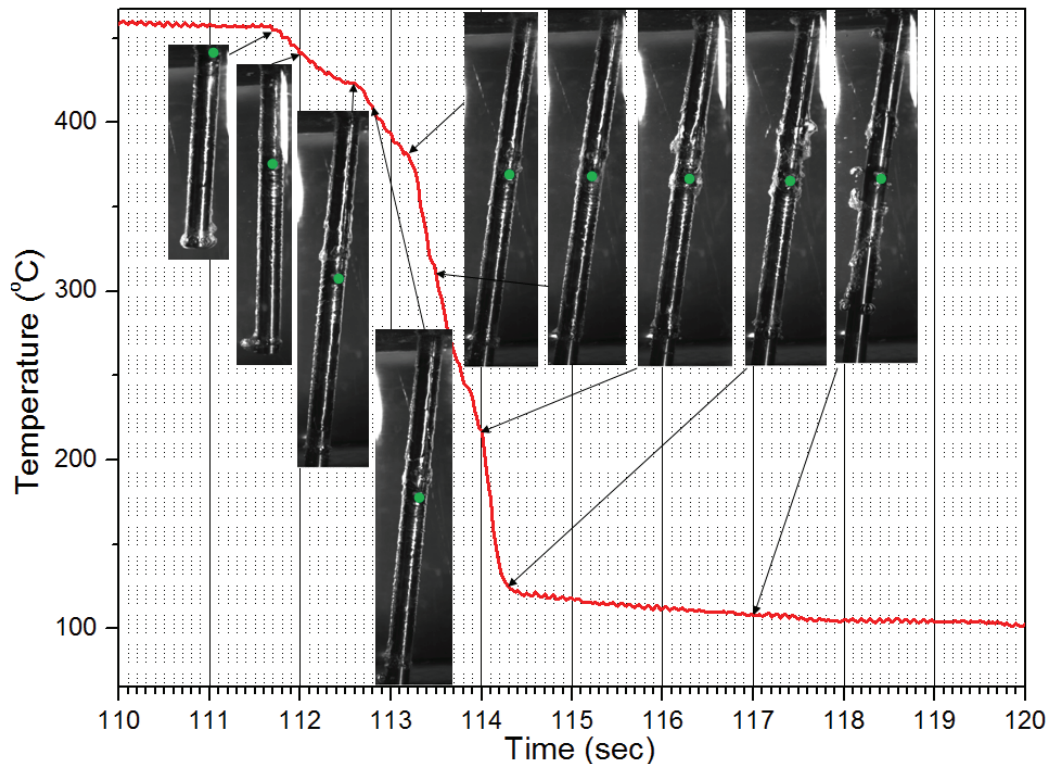


Figure 4. Temperature vs. time data during quenching in a saturated pool. Thermocouple location is shown as the green dot.

A distinct vapor film is observed which grows as time progresses. The interface then becomes wavy, with larger waves towards the upper region of the rod. This may be due to incremental increase in the mass of vapor in the film as we move upwards along the rod. The waves are seen to become larger in time. At 112.6 sec, somewhat larger waves are seen just above the thermocouple. Interestingly, there is also a sharper fall in temperature (implying greater heat transfer) beyond this point. At 112.86 sec, a small patch (encircled in fig. 5) was seen where water established contact with the rod surface. This was nearly at the same position where large waves were seen. The establishment of contact could be deduced from frothiness (fig. 5b, c) due to generation of bubbles. A patch of rewetting at the thermocouple was seen sometime later at ~113.07 sec. An increase in the rate of fall of temperature is also seen at ~113.2 sec. It is not very clear though whether these waves had any precursory role in establishment of water-surface contact.

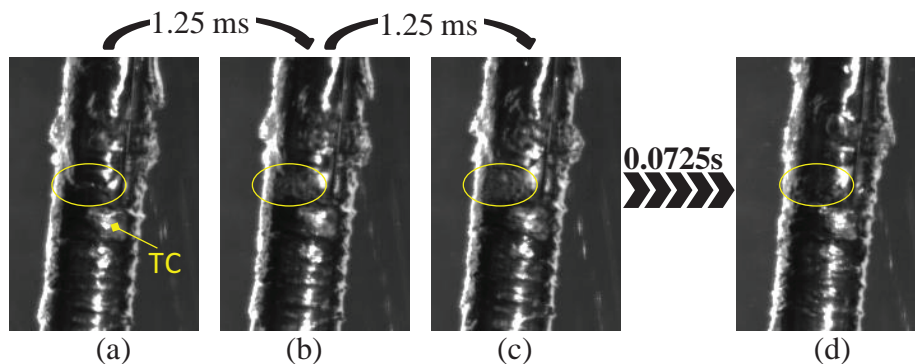


Figure 5. Intermittent patches of wetting and reforming of film. Film boiling existing at (a) gives way to a patch of contact (b) which grows (c). (d) Contact ceases and film boiling is reinstated.

It was observed that when water came into contact with the surface over a small region, boiling became very vigorous with bubbles nucleating at a very fast rate (fig. 5b, c). This continued for sometime till again the film formed over the surface only to be disrupted by another spell of vigorous boiling with water contacting the surface at a nearby patch. These patch wise contacts increased till the boiling became vigorous enough to disrupt the vapor film all around the periphery. In this regime, emission of numerous small bubbles is seen (fig. 6a). Such emission of small bubbles is also seen towards the lower side of the heater rod (fig. 6b) ahead of the quench front (shown approximately as the red line in fig. 6b) progressing upwards. The small bubbles are indicated by encircling them in the figure. The fact that these bubbles are very small is indicative of short intermittent contacts over small regions leading to formation and emission of small amount of vapor in the form of small bubbles.

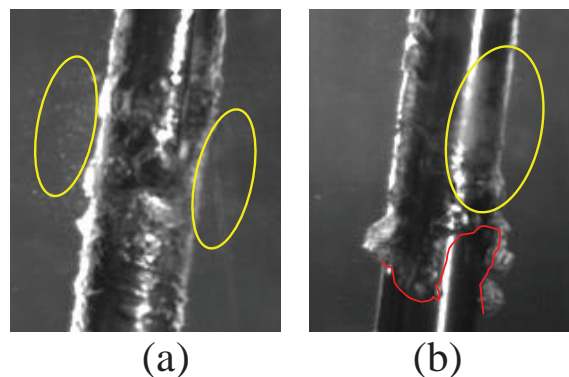


Figure 6. Transition boiling (a) near thermocouple location (b) near bottom of the rod

Fig. 6 characteristically shows transition boiling around the complete circumference. This is referred to a large scale transition boiling in this paper to distinguish it from small patches of vigorous boiling (fig. 5b, c). After this, peak heat flux is achieved. Finally large scale vapor generation ceases and nucleate boiling regime is achieved. It must be mentioned that the photographs of transition boiling are clearer on the lower side (fig. 6b) due to the fact that the heater is smooth on the lower end. The roughness generated due to the fixing of thermocouples is one of the reasons for more vigorous boiling and accelerated rewetting and quenching around the thermocouple location. In the present experiment, the quench front was seen to also spread out from the thermocouple location. Otherwise, one would have expected the wetting front only to move from bottom to top of the heater.

4.1.2. Subcooled pool

Quenching is much faster (as expected!) in the subcooled pool (fig. 7). The vapor film (if any) was not discernible but there was large amount of vapor generation in the form of numerous small bubbles as soon as the heater entered into the pool. Physically, this is similar to transition boiling regime encountered in the case of a saturated pool. Quenching could well be termed immediate with nucleate boiling initiating within ~0.5 sec of immersion. Phenomenology of the nucleate boiling regime was similar to saturated pool, but the rate of temperature fall was faster in the subcooled pool.

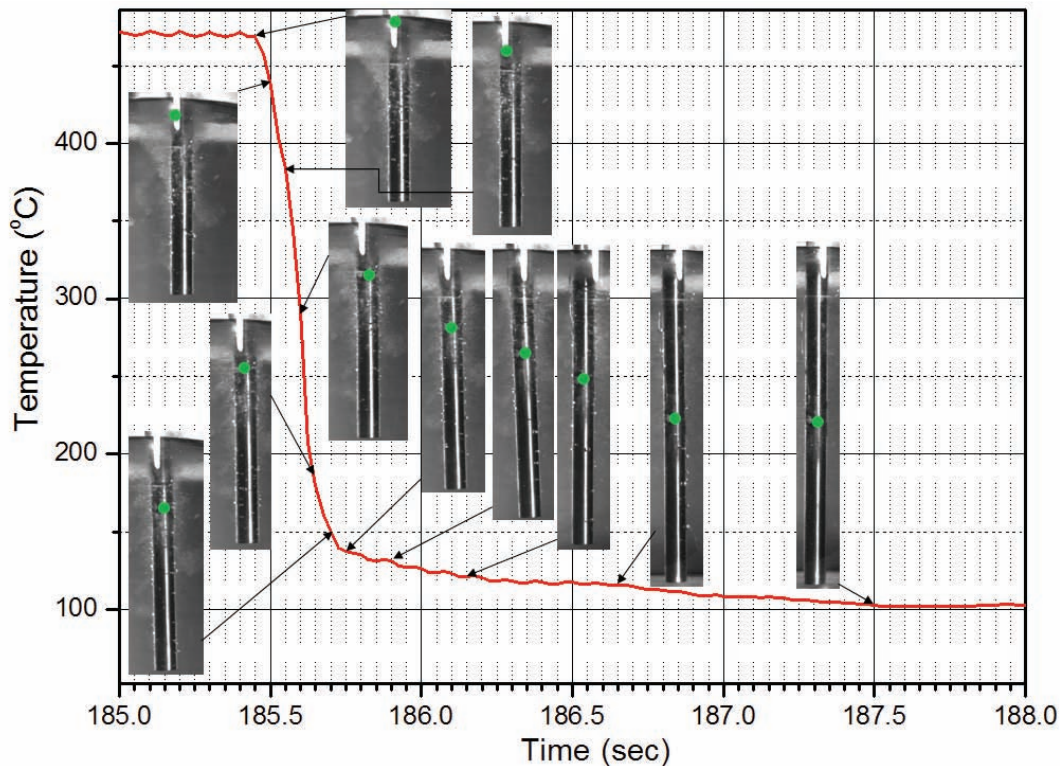


Figure 7. Temperature vs. time data during quenching in a subcooled pool. Thermocouple location is shown as the green dot.

4.1.3. Quenching time

The quenching curves for saturated and subcooled pool are re-plotted in fig. 8(a). The time scale is adjusted so that the immersion time at thermocouple location corresponds to 1 s. It is seen that the major temperature drop occurs for ~2.5 s in a saturated pool. In the subcooled pool apparently significant temperature drop occurs for ~0.3 s. This method of quantifying the quenching time is however subjective.

A more consistent estimate can be obtained by plotting the cooling rate and finding out the time for which negative values are obtained on the ordinate of fig. 8 (b). With this technique, the quenching time is seen to be 0.45 s for subcooled pool and 3.725 s for saturated pool. The cooling rate is significantly higher in the subcooled pool and shoots up as soon as immersion takes place. In the saturated pool, significant cooling rate is observed after ~ 1.5 s of immersion.

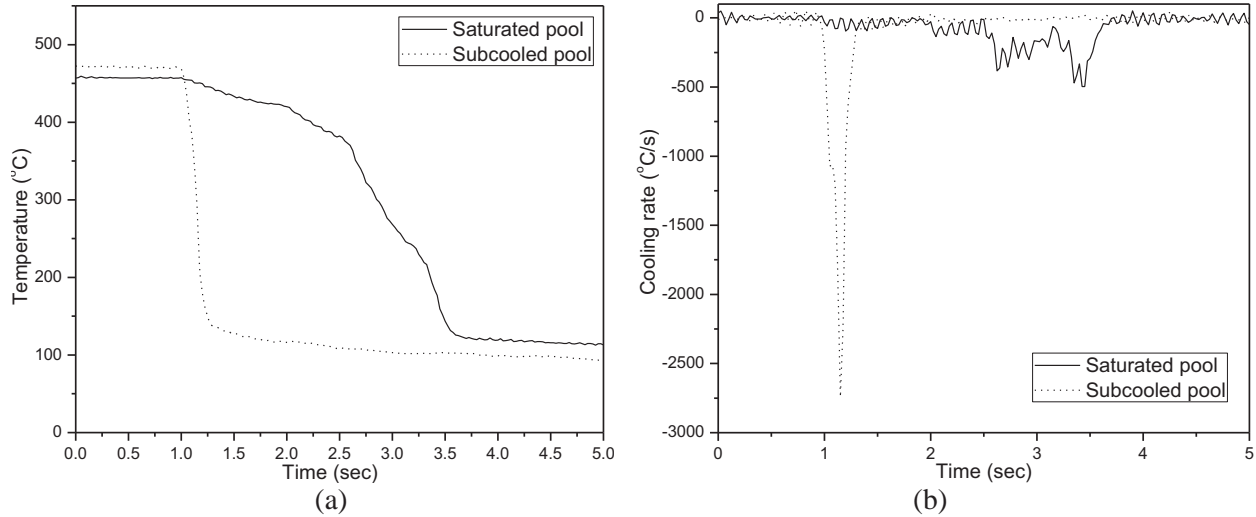


Figure 8. Comparison of quenching in subcooled and saturated pools: (a) quenching curve and (b) rate of cooling

4.2. Computed surface heat flux

The surface heat flux evaluated from the method outlined in section 3 help to gain additional insight into the physical phenomena. These curves when compared against the standard pool boiling curve [10] aid in identifying the different boiling regimes encountered during quenching.

4.2.1. Saturated pool

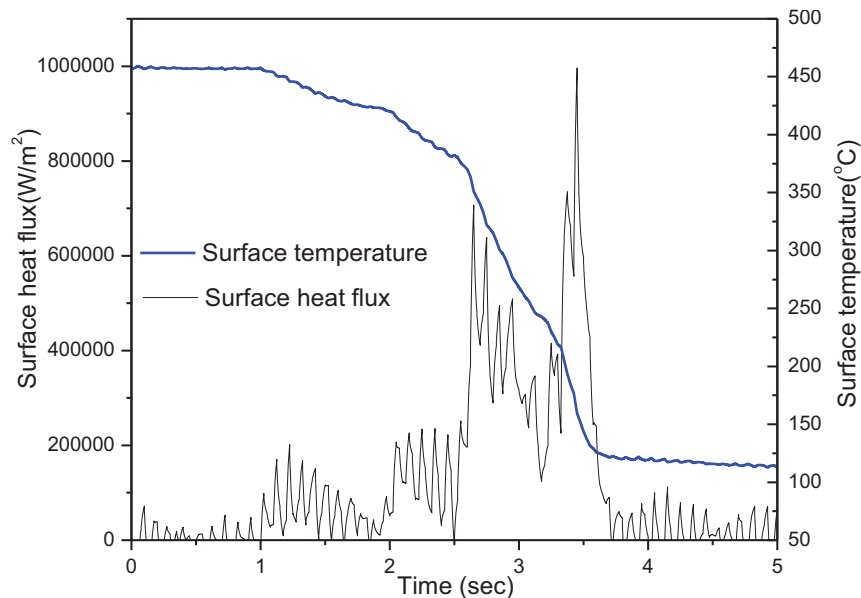


Figure 9. Surface heat flux in saturated pool

Figure 9 shows the derived surface heat flux for saturated pool. The time scale has been adjusted so that the immersion at thermocouple location starts at 1 sec. The temperature record is also plotted for reference. Immediately after immersion, the surface heat flux jumps. A similar jump is also seen at ~2 sec. The next jump is at ~2.5 sec. Beyond this, the curve bears striking resemblance to the standard pool boiling curve. In fact the peak heat flux of 1 MW/m^2 and rewetting temperature of 240°C are very close to saturated pool boiling values. The term peak heat flux is used in place of Critical Heat Flux (CHF), due to the importance of the term ‘CHF’ in nuclear safety, which is quite different from the present context. The timing of the transition boiling regime, characterized by increasing surface heat flux with reducing surface temperature, also matches with the time of the observation of large scale transition boiling in figure 6(a). However, the computed Minimum Heat Flux (MHF) of $\sim 0.1 \text{ MW/m}^2$ is substantially higher than saturated pool boiling MHF.

The computed heat flux shows fluctuations even prior to immersion. This is due to slight variations in thermocouple recordings. After the immersion, both the surface heat flux and its fluctuations increase. Based on the photographic observations and higher computed MHF, it can be concluded that film boiling is initiated as soon as the rod is immersed. However, due to relatively long duration ($\sim 0.08 \text{ sec}$) localized patches of rewetting and reinstating of film boiling, there are fluctuations in the heat flux. As the surface temperature falls, more such patches are activated thereby increasing heat flux. These patches result in heat flux during film boiling in the present case being an order of magnitude higher than pool boiling. It is postulated that as the number of patches increases, there is greater vapor generation. Since the surface is still hotter than rewetting temperature, a vapor film is again formed which then collapses only after the surface temperature falls below the rewetting temperature. It must be mentioned that similar patches were not seen towards the bottom of the heater where the surface is smooth. Thus the surface temperature and heat flux might be different on a smooth surface, at least in the film boiling regime.

4.2.2. Subcooled pool

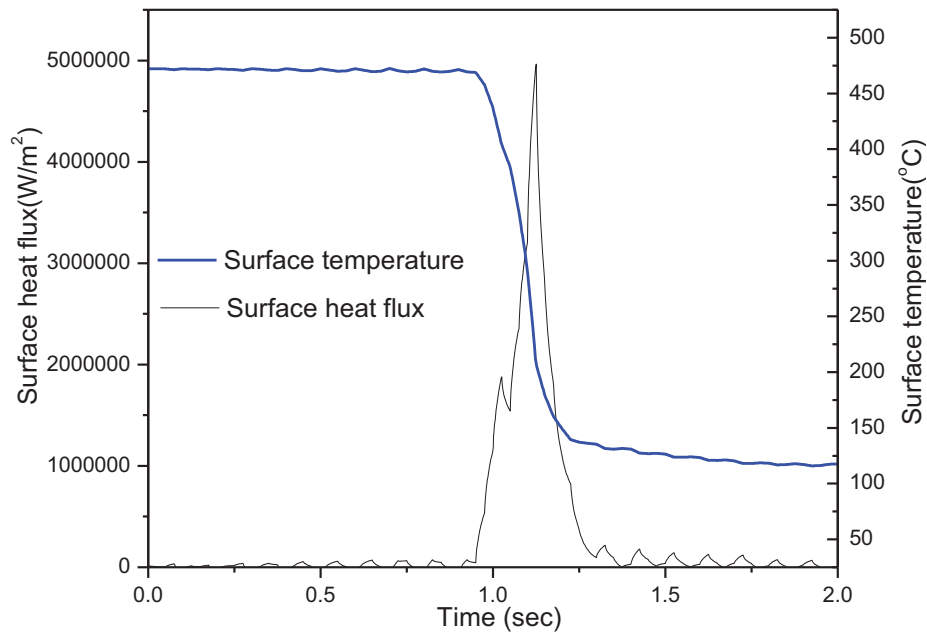


Figure 10. Surface heat flux in saturated pool

The surface heat flux results for the subcooled pool are shown in figure 10. Here, the computed heat flux is very smooth. There is apparently a very small time span ($\sim 1.0\text{-}1.05 \text{ sec}$) in which the characteristics of surface heat flux are analogous to film boiling. Beyond this, the transition and nucleate boiling regimes

are encountered. This is vindicated by the photographs where predominantly transition boiling type characteristics are observed. The peak heat flux is $\sim 5 \text{ MW/m}^2$ and rewetting temperature is $\sim 380^\circ\text{C}$. The absence of fluctuations during quenching also indicates that localized surface roughness does not influence the heat transfer in a subcooled pool.

The surface heat flux vs. surface temperature for the saturated and subcooled pools is plotted in fig. 11. The different boiling regimes in the saturated pool have been demarcated based on the visual observations. The curve is seen to resemble the pool boiling curve closely. The boiling regimes in subcooled pool are identified based on resemblance with the pool boiling curve as not much could be ascertained visually. The peak heat flux in subcooled pool is seen to be about 5 times higher than in a saturated pool.

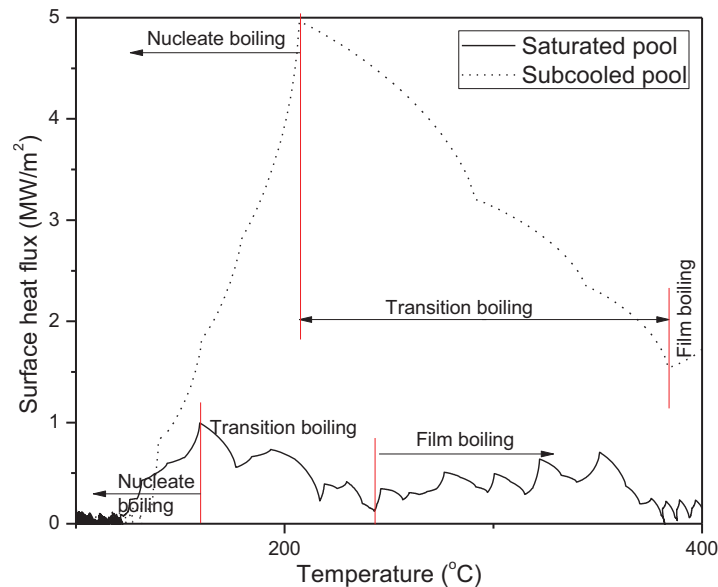


Figure 11. Surface heat flux versus surface temperature plot: effect of pool temperature

5. CONCLUSIONS

Experiments have been performed to study the phenomena occurring as a rod heated to around 470°C is immersed in a pool of water. The effect of pool temperature has been studied. Surface heat flux was computed from a measurement of single surface mounted thermocouple.

It was found that boiling curve similar (but not identical) to saturated pool boiling is retraced when quenching in a saturated pool. The values of peak heat flux and rewetting temperature obtained from heat flux computations were similar to pool boiling. Film boiling was observed for a substantial amount of time and the film boiling heat flux was an order of magnitude higher than pool boiling. This was postulated to be due to vapor film being interspersed with isolated patches of wetting and de-wetting prior to large scale transition boiling. Such patches were however not observed in the lower region of the rod. This was due to the lower end of the rod being smooth while fixing of the thermocouple had changed the surface characteristics at thermocouple location. Rewetting and quenching was seen to be accelerated at the thermocouple location.

In the subcooled pool, film boiling was not observed and the high speed photographs revealed phenomena which bear resemblance to transition boiling. This is also vindicated by surface heat flux calculations

which show a very small film boiling zone. The peak heat flux and wetting temperature are enhanced by 5 times and $\sim 140^{\circ}\text{C}$ respectively as compared to the saturated pool.

The surface heat flux vs. surface temperature data generated in this work can be used in models for heat transfer during quenching.

REFERENCES

1. E.K. Kalinin, I.I. Berlin, V.V. Kostiouk, "Transition Boiling Heat Transfer," *Advances in Heat Transfer*, **18**, 241–323 (1987).
2. General film boiling heat transfer prediction methods for advanced water cooled reactors, in: *Thermohydraulic Relationships Advanced Water Cooled Reactors*, IAEA-TECDOC-1203, (2001).
3. W.J. Chen, Y. Lee, D.C. Groeneveld, "Measurement of boiling curves during rewetting of a hot circular duct," *International Journal of Heat Mass Transfer*, **22**, 973–976 (1979).
4. J. Zhang, F. Tanaka, M. Juarsa, K. Mishima, "Calculation of boiling curves during rewetting of a hot vertical narrow channel," *Proceedings of NURETH-10*, Seoul, Korea (2003).
5. H. Kim, G. DeWitt, T. McKrell, J. Buongiorno, L. Hu, On the quenching of steel and zircaloy spheres in water-based nanofluids with alumina, silica and diamond nanoparticles, *International Journal of Multiphase Flow*, **35**, 427–438 (2009).
6. H. Kim, J. Buongiorno, L.W. Hu, T. McKrell, "Effect of nanoparticle deposition on rewetting temperature and quench velocity in experiments with stainless steel rodlets and nanofluids," *Proceedings of Seventh Int. ASME Conf. Nanochannels, Microchannels Minichannels*, Pohang, South Korea (2009).
7. D. Ciloglu, A. Bolukbasi, "The quenching behavior of aqueous nanofluids around rods with high temperature," *Nuclear Engineering and Design*, **241**, 2519–2527 (2011).
8. S.P. Walker, M. Ilyas, G.F. Hewitt, "The rewetting of PWR fuel cladding during post-LOCA reflood: a proposed physical explanation for the micro-scale high-frequency sputtering observed," *Proc. IMechE Part A: J. Power Energy*, **226**, 384–397 (2011).
9. A.K. Vishnoi, D.K. Chandraker, A.K. Pal, A. Dasgupta, P.K. Vijayan, D. Saha, "Design and development of 3 MW power rating directly heated 54-Rod fuel rod cluster simulator," *BARC/2010/R004*, Mumbai, India (2010).
10. S. Nukiyama, "Maximum and minimum values of heat q transmitted from metal to boiling water under atmospheric pressure," *International Journal of Heat Mass Transfer*, **9**, 1419–1433 (1965).